Coupling light to periodic nanostructures

Driessen, E.F.C.

Chapter 5

Enhanced coupling between plasmons in hole arrays with periodic dielectric antennas

We compare the angle-dependent transmission spectra of a metal hole array with dielectric pillars in each hole with that of a conventional metal hole array. The pillars enhance the optical transmission as well as the interaction between surface-plasmon modes. This results in an observed splitting $\Delta\omega/\omega$ as large as 6%, at normal incidence, for the modes on the pillar side of the array.

This chapter is based on D. Stolwijk, E. F. C. Driessen, M. A. Verschuuren, G. W. 't Hooft, M. P. van Exter, and M. J. A. de Dood, *Enhanced coupling of plasmons in hole arrays with periodic dielectric antennas*, Opt. Lett. **33**, 363–365 (2008).

5.1 Introduction

Metal films perforated with an array of subwavelength holes have intrigued researchers ever since the discovery that these arrays show extra-ordinary transmission of light [50]. It is generally accepted that the enhanced transmission is mediated by surface plasmons, electro-magnetic surface waves that are bound to a metal-dielectric interface. On a smooth interface these waves cannot be excited directly because their momentum is larger than that of light incident from the dielectric. Diffraction from a regular array of holes enables efficient excitation of the plasmon modes and increases the optical transmission. Due to this surface-plasmon excitation, the transmission of the hole array exceeds that, what is expected based on the transmission through a set of independent single holes [51].

The transmission spectra of metal hole arrays show a number of asymmetric resonances that correspond to different diffraction orders. Each of the resonances can be labeled by a specific reciprocal lattice vector [52]. The asymmetric lineshape of the resonances can be explained in terms of a phenomenological (Fano) model [29, 53–55]. Each peak features a maximum in transmission and a profound minimum, known as Wood's anomaly [56]. The frequencies of these features depend on the angle of incidence and can be compared to the dispersion relation of a plasmon on a smooth surface, folded back to the first Brillouin zone of the periodic lattice [52].

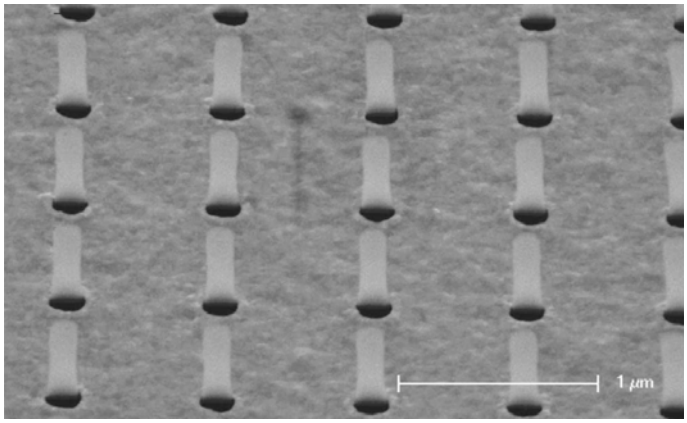

Figure 5.1. SEM image of the metal hole array created using an imprinting technique. The holes are 132 nm in diameter and each hole contains a ∼650 nm long glass pillar. The array has a lattice constant $a = 760$ nm.

In this chapter we study the polarization-dependent transmission spectra of metal films perforated with a square lattice of subwavelength holes. We compare the transmission of an array with a dielectric pillar in each of the holes with that of a conventional hole array. Transmission spectra of conventional hole arrays have been studied previously [57,58], and show that different modes can be excited depending on the input polarization. The p-polarized input light dominantly excites plasmon modes which propagate in the direction parallel and anti-parallel to the projected wave vector of the incident light. For small angles of incidence, coupling to modes that propagate in the approximately orthogonal direction is inefficient. We show that the excitation of these modes is strongly enhanced for the hole array with pillars. The pillars in the holes act as antennas that enhance the coupling to these modes. This provides a way of controlling the interaction between light and surface-plasmon modes.

5.2 Experiment

The metal hole arrays in the experiment were made using an imprinting technique. An array of pillars was defined by e-beam lithography and was used to create a rubber stamp. A replica of the array was created by pressing the stamp into a layer of liquid sol-gel glass. This second array was then coated with a layer of gold. The gold was selectively removed from the pillars with a wet etch, by making use of the fact that the gold layer deposited on the side of the pillars is thinner than the layer on the substrate. The result is a metal hole array with a $\sim$650 nm long glass pillar sticking out of each hole, as shown in Fig. 5.1. The 0.5×0.5 mm^2 array was created on an AF45 glass substrate with $n \approx 1.52$. A 100 nm thick layer of sol-gel glass with a refractive index $n \approx 1.41$ was left between the substrate and the gold layer. The gold layer is 200 nm thick and is perforated by a square array of pillars with a lattice constant $a = 760\pm4$ nm* and a diameter $d = 135\pm5$ nm. After measuring the transmission of this array, we selectively removed the glass pillars using hydrofluoric acid, to create a conventional hole array, and repeated the transmission measurement.

The optical transmission of the hole array was measured using an incandescent lamp coupled to a 200 μm multimode optical fiber. A set of lenses was used to create a $\sim$300 μm diameter spot on the sample. The transmitted light was sent to a fiber-coupled grating spectrometer with a CCD detector (resolution 1.2 nm) to measure the spectral content. Apertures limited the numerical aperture of the incident and transmitted light beam to less than

*The lattice constant was obtained from diffraction measurements with an He-Ne laser.

0.01. Polarizers were placed in parallel parts of the incident and transmitted beam to control the polarization. To measure the angular dispersion, the substrate was placed on a rotation mount with the rotation axis aligned to the $(0, 1)$-direction of the hole array. The wave vector of the incident light was in the plane perpendicular to this direction.

Figure 5.2 shows measured transmission spectra (normalized to the lamp spectrum) of the metal hole array both before (dashed lines) and after (solid lines) removing the pillars. Spectra are shown for normal incidence (bottom) and 15° angle of incidence (top). The maximum transmission decreases, and at the same time the resonance narrows while the maximum shifts to shorter wavelengths. The observed change in line shape corresponds to a Fano resonance for which the amplitudes of both the direct and resonant channel, as well as the linewidth of the resonance, are reduced by a factor 2. Note that the spectral positions of the transmission minima do not shift when the hole size is reduced [56, 59]. The marginal shift that we do observe is attributed to the fact that the pillars change the effective index of the surface plasmon.

5.3 Coupling to surface plasmons

Each resonance in the transmission spectra can be labeled with a specific reciprocal lattice vector. The labels (i, j) in Fig. 5.2 refer to the reciprocal lattice vector $\vec{G} = i\vec{G}_{\mathrm{x}} + j\vec{G}_{\mathrm{y}}$, where $\vec{G}_{\mathrm{x,y}}$ are the two basis vectors of the reciprocal lattice. The condition for exciting a surface-plasmon mode is given by:

$$\vec{k_{\parallel}} = \vec{k}_{\mathrm{SP}} + \vec{G}, \tag{5.1}$$

where $\vec{k}_{\parallel}$ is the projection of the wave vector of the incoming light onto the metal-dielectric interface, and $\vec{k}_{\mathrm{SP}}$ is the propagation constant of the surface plasmon. To describe the dispersion, we approximate the propagation constants of the surface plasmons on both sides of the metal hole array with that of a plasmon on a smooth metal-dielectric interface:

$$k_{\mathrm{SP}}(\omega) = \frac{\omega}{c}\left(\frac{\epsilon_{\mathrm{d}}\epsilon_{\mathrm{m}}(\omega)}{\epsilon_{\mathrm{d}} + \epsilon_{\mathrm{m}}(\omega)}\right)^{1/2}, \tag{5.2}$$

where c is the speed of light, ϵ_{d} is the dielectric constant of the dielectric and $\epsilon_{\mathrm{m}}(\omega)$ is the frequency-dependent dielectric constant of the metal.

Figure 5.3 shows grayscale plots of the transmission as a function of the angle of incidence (horizontal axis) and the wavelength (vertical axis) for the sample without pillars (top) and with pillars (bottom). The dark bands in

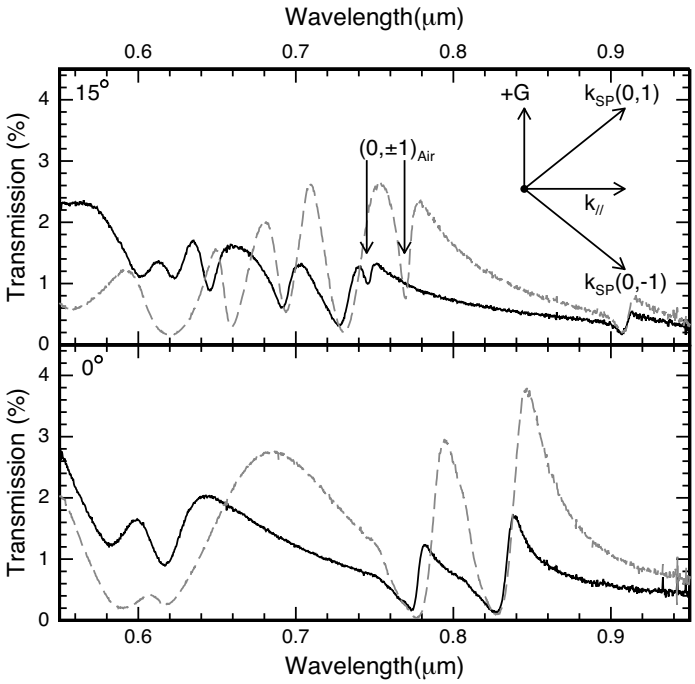

Figure 5.2. Transmission spectra of a conventional metal hole array (solid curve) and a metal hole array with pillars (dashed curve), for p-polarized light. Spectra are shown for normal incidence (bottom) and 15° angle of incidence (top). The arrows indicate the $(0, \pm 1)$ resonance for 15° angle of incidence. The inset shows the wavevector $\vec{k}_{\parallel}$, a reciprocal lattice vector $\vec{G}$ in the (0,1) direction and the propagation direction of the two (0,±1) surface-plasmon modes.

the figure correspond to the minima in the transmission spectra. The white curves are the frequencies calculated from Eqs. (5.1) and (5.2) for different reciprocal lattice vectors $\vec{G}$, using the tabulated frequency dependence of the dielectric constant of gold [60], and an effective index of $n \approx 1.46$ for the glass substrate*. A distinction is made between surface-plasmon modes on the air side (dashed curves) and on the glass side (solid curves). The $(\pm 1, 0)$ and $(0, \pm 1)$ modes on the air side are degenerate at normal incidence. When the angle of incidence is changed, the degeneracy is lifted and the resonance splits into a $(1, 0)$, a $(-1, 0)$, and a degenerate $(0, \pm 1)$ resonance. The $(1, 0)$ and $(-1, 0)$ modes have a strong dispersion, because $\vec{k}_{\parallel}$ and $\vec{G}$ are parallel. For the

*The effective index is based on the calculated propagation constant of a surface plasmon on an interface of gold with a 100 nm layer of sol-gel glass.

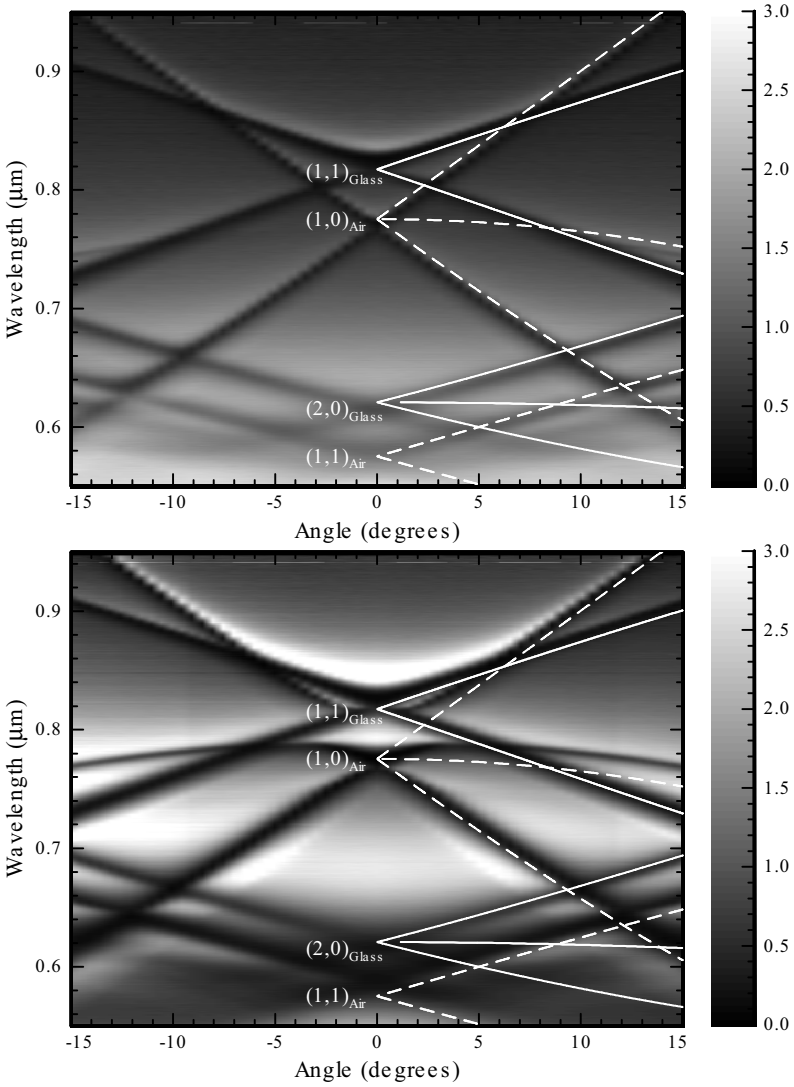

Figure 5.3. Grayscale plots of the measured transmission as a function of angle of incidence and wavelength, for the metal hole array without pillars (top) and with pillars (bottom). The grayscale ranges from 0 to 3% transmission. The white curves indicate the frequencies calculated from Eqs. (5.1) and (5.2). The solid curves are for modes on the glass side, while the dashed curves are for modes on the air side.

$(0, \pm 1)$ modes the dispersion is limited, because $\vec{k_{\|}}$ and $\vec{G}$ are perpendicular. For the conventional array the $(0, \pm 1)$ resonance is barely visible for small angles, consistent with earlier work [58]. The resonance is strikingly visible in the transmission of the array with pillars. The large difference in amplitude for this resonance is also clearly visible in the top part of Fig 5.2 (arrows).

For the geometry of our structure, the scattering plane coincides with a (1,0) direction of the square lattice. This plane is a mirror plane of the hole array, and the modes can be classified as either *odd* or *even* relative to this plane. The *p*-polarized input light has an *odd* H-field distribution relative to this plane, and therefore only plasmon modes with an *odd* H-field distribution can be excited. At normal incidence, this corresponds to plasmon modes that propagate in the direction of the E-field vector [61], i.e. the $(\pm 1, 0)$ directions. For finite angles of incidence it is possible to couple to a combination of $(0, \pm 1)$ modes. The direction of propagation of these modes is sketched in the inset of Fig. 5.2. The pillars in the holes do not change the symmetry, but act as antennas and affect the efficiency with which the modes are excited. The interaction between light and a dielectric pillar is strongest when the E-field is parallel to the long axis of the pillars. As a result, when pillars are placed in the holes, the coupling to the $(0, \pm 1)$ modes on the air side is enhanced for *p*-polarized light.

5.4 Coupling between surface plasmons

For both arrays, the angle dependent transmission in Fig. 5.3 shows that the $(\pm 1, 0)$ air modes have an almost-linear dispersion at sufficiently large angles of incidence. For smaller angles, this only holds for the conventional hole array. For the hole array with pillars, the $(\pm 1, 0)$ modes on the air side are clearly coupled. At normal incidence we observe two minima in the spectra at 775 and 825 nm. The minimum at 825 nm coincides with the minimum of the $(1, 1)$ glass modes. At normal incidence, the excited plasmon modes are standing waves. The resonances occur at different energies depending on the position of the nodes and anti-nodes of the standing waves relative to the holes [36, 54]. Without pillars, this energy difference is small and the splitting is not resolved. The pillars lower the energy only of the mode that has anti-nodes at the position of the pillars. For our array, with a filling factor of pillars of only 2.3%, this leads to an observed splitting of the resonances of 6% of the center frequency. Note that we used the separation between the minima as a measure of the splitting, because the minima do not shift when radiation losses are increased [56, 59]. We have compared this splitting to a two-band

model and to a model that uses the polarizability per unit volume. We find that the calculated splitting from these simplified models is much smaller than the observed splitting.

Increasing the filling factor of pillars will certainly increase the energy difference between the modes. However, a larger hole size also leads to larger radiation losses [54], and broadens the spectral features. This may obscure the effect. Similar effects are expected when dielectric hole arrays are placed on top of a metal hole array, although the interaction with p-polarized light is generally weaker, when compared to pillars. This kind of hybrid structures can be used to (locally) tune the dispersion of the surface modes of a metal film. By locally adding or removing pillars (holes), control of the excitation and propagation of plasmons on the wavelength scale can be achieved. When the interaction between plasmon modes can be increased, it becomes conceivable that two-dimensional periodic metal-dielectric structures exist that do not allow coupling of light waves to surface modes in any direction, for a certain range of frequencies. This effect would be analogous to the existence of photonic bandgaps in two-dimensional dielectric structures.